Article

Topotactic Oxidative and Reductive Control of the Structures and Properties of Layered Manganese Oxychalcogenides

Geoffrey Hyett, Nicolas Barrier, Simon J. Clarke, and Joke Hadermann

J. Am. Chem. Soc., **2007**, 129 (36), 11192-11201• DOI: 10.1021/ja073048m • Publication Date (Web): 18 August 2007

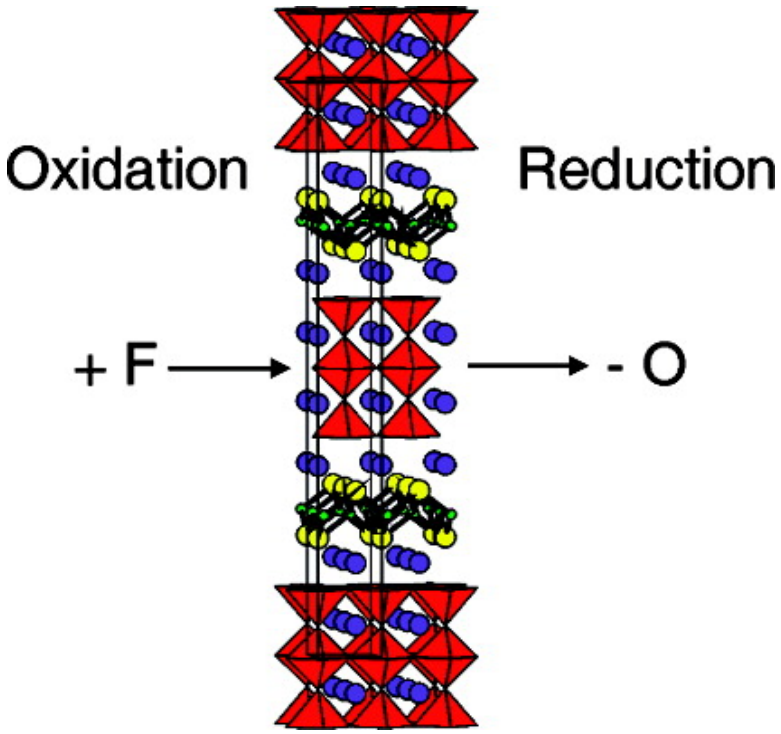

More About This Article

Additional resources and features associated with this article are available within the HTML version:

- Supporting Information
- Links to the 5 articles that cite this article, as of the time of this article download
- Access to high resolution figures
- Links to articles and content related to this article
- Copyright permission to reproduce figures and/or text from this article

J|A|C|S
ARTICLES
Published on Web 08/18/2007

Topotactic Oxidative and Reductive Control of the Structures and Properties of Layered Manganese Oxychalcogenides

Geoffrey Hyett,[†] Nicolas Barrier,[†] Simon J. Clarke,*[,†] and Joke Hadermann[‡]

Contribution from the Department of Chemistry, University of Oxford, Inorganic Chemistry Laboratory, South Parks Road, Oxford, OX1 3QR, U.K., and Electron Microscopy for Materials Science (EMAT), University of Antwerp, Groenenborgerlaan 171, B-2020 Antwerp, Belgium

Received May 1, 2007; E-mail: simon.clarke@chem.ox.ac.uk

Abstract: Topotactic modification, by both oxidation and reduction, of the composition, structures, and magnetic properties of the layered oxychalcogenides $Sr_4Mn_3O_{7.5}Cu_2Ch_2$ (Ch = S, Se) is described. These Mn^{3+} compounds are composed of alternating perovskite-type strontium manganese oxide slabs separated by anti-fluorite-type copper chalcogenide layers and are intrinsically oxide deficient in the central layer of the perovskite slabs. The systems are unusual examples of perovskite-related compounds that may topotactically be both oxidized by fluorination and reduced by deintercalation of oxygen from the oxide-deficient part of the structure. The compounds exhibit antiferromagnetic ordering of the manganese magnetic moments in the outer layers of the perovskite slabs, while the other moments, in the central layers, exhibit spin-glass-like behavior. Fluorination has the effect of increasing the antiferromagnetic ordering temperature and the size of the ordered moment, whereas reduction destroys magnetic long-range order by introducing chemical disorder which leads to both further disorder and frustration of the magnetic interactions in the manganese oxide slab.

Introduction

In recent years there has been considerable interest in manganite oxide compounds which exhibit the phenomenon of colossal magnetoresistance in which the onset of ferromagnetic ordering coincides with a dramatic increase in electrical conductivity, and thus provides systems with electronic transport properties which are sensitive to an applied magnetic field. The oxides explored in this context are mainly perovskites $(A_{1-x}A'_x)MnO_3$ in which A and A' are normally divalent and trivalent cations of electropositive metals,[1,2] and Ruddlesden−Popper (R−P) phases $(A_{1-x}A'_x)_{n+1}Mn_nO_{3n+1}$, for which n is usually ≤ 3 and for which the $n = \infty$ member is perovskite itself,[3] and brownmillerites such as $SrCaMnGaO_{5+\delta}$.[4] These compounds contain manganese in oxidation states between +3 and +4, and considerable recent study has focused on the still-controversial issues of charge and orbital ordering in these compounds to fully explain the properties.[5−7]

The R−P oxides may be considered intergrowths of blocks of the cubic perovskite structure n layers of octahedra thick separated by AO layers which resemble slabs of the rock-salt structure. Recently, a number of more complex intergrowth phases have been isolated in which perovskite-type oxide blocks are separated by antifluorite-type slabs $M'_{2m}E_{m+1}$ (m = 1, 2, 3) in which M' is usually a late transition metal or a main group metal and is tetrahedrally coordinated by a non-oxide anion E which is usually a chalcogenide[8−12] or pnictide[13] anion. These phases are most widely represented by oxychalcogenides in which the anti-fluorite layer is composed of Cu^+ ions in tetrahedral coordination by chalcogenide anions. Figure 1 compares the idealized $n = 3$ R−P structure, represented, for example, in this ideal form by $Sr_4Ti_3O_{10}$[14] and in a distorted form by $Ca_4Mn_3O_{10}$,[15] and the structure of the oxychalcogenides $Sr_4Mn_3O_{8-\delta}Cu_2Ch_2$ (Ch = S, Se; $\delta = 0.5$) first described by Zhu and Hor[8] which are the subject of this paper. Because the synthetic conditions for chalcogenide-containing phases must be anaerobic and because the chalcogens are less oxidizing than oxygen, lower transition metal oxidation states may be stabilized in the mixed-anion phases than are commonly found in pure oxide analogues. The previously reported compounds $Sr_4Mn_3O_{7.5}Cu_2Ch_2$ (Ch = S, Se)[8] contain Mn^{3+} ions resulting in an intrinsic anion-deficiency, whereas oxidation states as high

[†] University of Oxford.
[‡] University of Antwerp.

(1) Jin, S.; Tiefel, T. H.; McCormack, M.; Fastnacht, R. A.; Ramesh, R.; Chen, L. H. *Science* **1994**, *264*, 413.
(2) Raveau, B.; Maignan, A.; Martin, C.; Hervieu, M. *Chem. Mater.* **1998**, *10*, 2641.
(3) Battle, P. D.; Rosseinsky, M. J. *Curr. Opin. Solid State Mater. Sci.* **1999**, *4*, 163.
(4) Battle, P. D.; Bell, A. M. T.; Blundell, S. J.; Coldea, A. I.; Gallon, D. J.; Pratt, F. L.; Rosseinsky, M. J.; Steer, C. A. *J. Solid State Chem.* **2002**, *167*, 188.
(5) Rao, C. N. R.; Arulraj, A.; Cheetham, A. K.; Raveau, B. *J. Phys.: Condens. Mater.* **2000**, *12*, R83.
(6) Goff, R. J.; Attfield, J. P. *Phys. Rev. B.* **2004**, *70*, 140404(R).
(7) Attfield, J. P. *Solid State Sci.* **2006**, *8*, 861.
(8) Zhu, W. J.; Hor, P. H. *J. Solid State Chem.* **2000**, *153*, 26.
(9) Zhu, W. J.; Hor, P. H.; Jacobson, A. J.; Crisci, G.; Albright, T. A.; Wang, S.-H.; Vogt, T. *J. Am. Chem. Soc.* **1997**, *119*, 12398.
(10) Zhu, W. J.; Hor, P. H. *J. Solid State Chem.* **1997**, *130*, 319.
(11) Gál, Z. A.; Rutt, O. J.; Smura, C. F.; Overton, T. P.; Barrier, N.; Clarke, S. J.; Hadermann, J. *J. Am. Chem. Soc.* **2006**, *128*, 8530.
(12) Zhu, W. J.; Hor, P. H. *J. Solid State Chem.* **1997**, *134*, 128.
(13) Brock, S. L.; Raju, N. P.; Greedan, J. E.; Kauzlarich, S. M. *J. Alloys Compd.* **1996**, *237*, 9.
(14) Ruddlesden, S. N.; Popper, P. *Acta Crystallogr.* **1958**, *11*, 54.
(15) Battle, P. D.; Green, M. A.; Lago, J.; Millburn, J. E.; Rosseinsky, M. J.; Vente, J. F. *Chem. Mater.* **1998**, *10*, 658.

10.1021/ja073048m CCC: $37.00

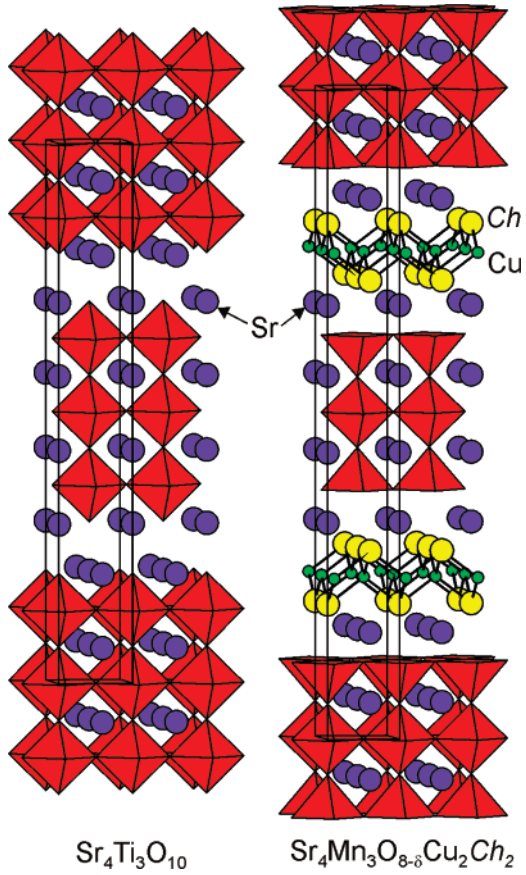

Figure 1. Comparison of the $n = 3$ Ruddlesden−Popper structure type of $Sr_4Ti_3O_{10}$ (left)[14] and the structures of the oxychalcogenides $Sr_4Mn_3O_{7.5}Cu_2Ch_2$ (Ch = S, Se) described in this paper (right). Formally, in deriving the structures of the oxychalcogenides, the oxide ions in the rock-salt-type layers of the $Sr_4Ti_3O_{10}$ structure are replaced by chalcogenide ions, and additional copper ions occupy tetrahedral sites in these layers which are coordinated by chalcogenide ions. MnO_5, MnO_6, and TiO_6 polyhedra are shown.

as +4 for Mn may readily be obtained in manganite perovskite and R−P oxide phases. In this paper we demonstrate that the anion content and hence the Mn oxidation state in $Sr_4Mn_3O_{7.5}Cu_2Ch_2$ (Ch = S, Se) may be controlled by postsynthetic low-temperature fluorination (using XeF_2[16,17]) or reduction (using NaH[18]), resulting in significant changes in the structural details and the magnetic ordering which correlate smoothly with composition.

Experimental Section

Synthesis. With the exception of the reduced oxychalcogenides which readily undergo aerial reoxidation, the products reported are air stable. However, one or more moisture-sensitive reactants was invariably involved, so manipulations of solids were carried out in a Glove Box Technology argon-filled recirculating dry box with a combined O_2 and H_2O content of less than 5 ppm. The following starting materials were used as supplied: MnO_2 powder (ALFA 99.999%), Cu powder (ALFA 99.9995%), Mn flake (Aldrich 99.98%) cleaned with 15% nitric acid in methanol and ground into powder in the glove box, CuO powder (Aldrich 99.99%), Se shot (Alfa 99.999%) ground into powder, XeF_2 crystals (Alfa, 99.5%), and NaH powder (Aldrich 95%). SrS was synthesized by the reaction at 900 °C for 8 h between $SrCO_3$ (ALFA 99.994%) powder and CS_2 (Aldrich 99.5%) vapor which was carried over the hot carbonate by a stream of argon (BOC, Pureshield). (**Caution: CS_2 is toxic and highly flammable: the apparatus was contained in a fumehood, and excess CS_2 was hydrolyzed using a hydroxide bleach bubbler located downstream of the reaction**!) Cu_2S was prepared by reacting copper powder with sulfur (ALFA 99.9995%) in a dried, evacuated, sealed silica tube at 700 °C for 3 days. The temperature was raised slowly between 400 and 700 °C after a 12 h soak at 400 °C in order to avoid a buildup of sulfur pressure. SrO was prepared by decomposing $SrCO_3$ under dynamic vacuum at 900 °C for 24 h with a final firing of 3 h at 1100 °C. $SrCuO_2$ was prepared by reacting $SrCO_3$ with CuO powder at 1000 °C in air. Purities were assessed using powder X-ray diffraction (PXRD).

For the high-temperature synthesis of oxychalcogenides the reactants were mixed thoroughly in an agate pestle and mortar, pressed into a pellet at 150 MPa, and placed in a dry alumina crucible inside a silica tube that had been baked dry under vacuum for 2−3 h at 1000 °C prior to loading in the dry box. The tube was sealed under vacuum (10^{-2} mbar) and heated in an electrical resistance chamber furnace. Initially, single crystals (black platelets) with a formula derived from the single-crystal analysis of $Sr_4Mn_{2.94(1)}Cu_2O_{7.42(5)}S_2$ were obtained along with other products[19] by heating 1.5 g of a mixture of MnO_2, SrO, SrS, Sr (Aldrich 99% and sublimed at 700 °C under 10^{-2} mbar), and Cu_2S in the molar ratio 2/1/1/1/1 at 1050 °C for 18 days. For the subsequent synthesis of pure $Sr_4Mn_{3-\gamma}O_{7.5-\epsilon}Cu_2S_2$ ($\gamma \approx \epsilon \approx 0.1, 0.2$) on the 10-g scale the reagents used were stoichiometric quantities of $SrCuO_2$, SrS, Mn, and MnO_2 (i.e., molar ratio 8/8/7/5). Intentional MnO-deficiency ($\gamma \approx \epsilon \leq 0.2$) in the reaction mixture was later introduced by reducing equally the molar amounts of Mn and MnO_2. $Sr_4Mn_3O_{7.5}Cu_2Se_2$ was synthesized by grinding together $SrCuO_2$, SrO, Se, MnO_2, and Mn powders in the molar ratio 8/8/8/3/9. No Mn-deficiency was indicated in this phase. Mixtures were reacted initially at 900 °C for 5−8 days and then at 1000 °C for one or two further periods of 5−8 days with intermediate regrinding in the glove box; the progress of the reactions was monitored by PXRD.

Batches of 8−10 g of the oxysulfides and oxyselenide were prepared so that fluorination and reduction reactions and subsequent analysis, including structural and magnetic investigations using neutron powder diffraction, could be carried out on portions of the same batch of material. Fluorination of the oxysulfide was carried out by gently grinding together 4 g of $Sr_4Mn_{3-\gamma}O_{7.5-\delta}Cu_2S_2$ with 0.25 mol equiv (0.216 g) of XeF_2 and sealing this mixture, using a homemade arc welding furnace, inside a 9-mm diameter nickel tube (wall thickness 0.45 mm) under argon which had been cleaned by passage over titanium turnings held at 800 °C. The Ni tube was sealed inside a glass tube for protection and heated at 225 °C for 5 days. In some cases further reactions using further 0.1 mol equiv portions of XeF_2 were performed to attempt to increase the fluorination level. Similar conditions were applied in the case of the oxyselenide. Higher temperatures or larger excesses of XeF_2 resulted in the formation of substantial amounts of SrF_2.

Oxidation of the oxysulfide was also attempted by exposing a sample of the material to O_2 gas at 130 bar and 100 °C. However, there was no measurable change in the powder pattern of the sample, suggesting that this oxidation route is not viable. Reduction was carried out using the hydride reduction method described in ref 18: 4 g of $Sr_4Mn_{3-\gamma}O_{7.5-\epsilon}Cu_2S_2$ was ground together with 0.15 mol equiv (0.018 g) of NaH. The mixture was sealed under vacuum (10^{-2} mbar) in a silica tube and heated at 180 °C for 5 days. This process was repeated with further additions of 0.15 and 0.1 mol equiv of NaH so that a total of 0.4 mol equiv of NaH was used. After this three-step reaction the product was washed three times with dry methanol to remove NaOH formed in the reduction and any unreacted NaH. This stepwise procedure adopted

(16) Ardashnikova, E. I.; Lubarsky, S. V.; Denisenko, D. I.; Shpanchenko, R. V.; Antipov, E. V.; Van Tendeloo, G. *Physica C* **1995**, *253*, 259.
(17) Greaves, C.; Francesconi, M. G. *Curr. Opin. Solid State Mater. Sci.* **1998**, *3*, 132.
(18) Hayward, M. A.; Green, M. A.; Rosseinsky, M. J.; Sloan, J. *J. Am. Chem. Soc.* **1999**, *121*, 8843.
(19) Barrier, N.; Clarke, S. J. *Chem. Commun.* **2003**, 164.

for the oxysulfides was required to avoid the formation of elemental copper by the reduction of Cu^+ ions in the chalcogenide layers which occurred if too much NaH was used or if the reaction temperature was higher than 180 °C. However, the reduced selenide was made in a single reaction step: 4 g of $Sr_4Mn_3O_{7.5}Cu_2Se_2$ was reacted with 0.2 mol equiv (0.0226 g) of NaH at 180 °C for 5 days and washed as described above. When the reductions were attempted using a 5% H_2/95% N_2 mixture at 200 °C, decomposition occurred with the formation of large amounts of elemental copper. Attempts to fluorinate the reduced materials were also unsuccessful as the reduced product was extremely reactive toward XeF_2 (reaction occurred spontaneously and vigorously on contact between XeF_2 and the reduced powder), and inhomogeneous products containing substantial amounts of SrF_2 were obtained.

Chemical Analysis. EDX analysis using a JEOL JSM-840A scanning electron microscope equipped with an Oxford Instruments ISIS300 energy dispersive X-ray analysis system was carried out on crystals of the oxysulfide to determine the approximate elemental content. Attempts to measure the Mn oxidation state using iodometric titration were hampered by the formation of Cu^{2+} which oxidizes I^-. Oxidative thermogravimetric analysis (TGA) carried out in air using a Rheometric Scientific STA 1500 instrument was hampered by the air-sensitivity of the reduced materials.

Powder X-ray Diffraction (PXRD). Measurements were made on Panalytical X'pert Pro and Siemens D5000 diffractometers using Cu $K\alpha_1$ radiation with the sample mounted on a glass slide. The air-sensitive reduced materials were contained within a homemade sealed sample holder.

Single-Crystal X-ray Diffraction (SXRD). Intensity data for a black platelet single crystal (0.06 × 0.03 × 0.01 mm^3) of $Sr_4Mn_{2.94(1)}Cu_2O_{7.42(5)}S_2$ were collected on a Nonius Kappa CCD diffractometer using graphite-monochromated Mo Kα radiation ($\lambda = 0.71073$ Å) at room temperature. The frames were recorded using $\Delta\omega = 1.20°$ rotation scans with an X-ray exposure time of 100 s per frame. Reflection indexing, Lorentz-polarization correction, peak integration, and background determination were performed using the program DENZO[20] of the Kappa CCD software package. An absorption correction, using a Gaussian integration method[21] based on the crystal shape, was applied to the reflection intensities. Structure solution using Direct Methods was performed using SIR97,[22] and all structure refinements were carried out using the SHELXL97[23] structural refinement program.

Powder Neutron Diffraction (PND). Two to four gram samples contained in 8-mm diameter vanadium cans (sealed in the glove box with indium gaskets in the case of the reduced materials) were measured at temperatures between 2 and 298 K on the diffractometer POLARIS at the ISIS Facility, Rutherford Appleton Laboratory, UK and on the instrument D2B at the Institute Laue-Langevin (ILL), Grenoble. On POLARIS diffraction patterns were measured by the time-of-flight method in the *d*-spacing range $0.5 < d < 8$ Å using detector banks at mean scattering angles 2θ of 35°, 90°, and 145°; typically, measurement was carried out such that the product of the sample mass, measuring time, and proton current at the production target was approximately 1000 μA h g. All measurements used for structural comparisons were made on POLARIS. On D2B neutrons with wavelengths of 1.59 or 2.39 Å were selected using a 28-crystal Ge(335) monochromator and were detected over the 2θ range 0−160° in steps of 0.05° for 5 s per point. Low-temperature data were collected down to 5 K with the samples in a closed-cycle helium refrigerator. Rietveld refinements were carried out using the GSAS suite[24] via the EXPGUI interface.[25] D2B data were used for analysis of the magnetic structures; form factors for magnetic scattering were taken from the International Tables for Crystallography.[26]

Electron Diffraction Measurements. Measurements were carried out on a Phillips CM20 transmission electron microscope with a LaB_6 filament.

Magnetic Susceptibility Measurements. Measurements were carried out using Quantum Design MPMS-5 or MPMS-XL SQUID magnetometers on approximately 50 mg of the same materials as were measured using neutron diffraction. Samples were contained in gelatin capsules, which in the case of the air-sensitive reduced materials were sealed with superglue immediately on removal from the glove box. The magnetic moments of the samples were measured as a function of temperature on warming in fields of 10 mT and 100 mT after cooling in zero field (zero-field cooled: ZFC) and then in the measuring field (field-cooled: FC). Magnetization isotherms were measured in the range ±5 T with cooling in a 5 T field.

Electrical Resistivity Measurements. Measurements were made on sintered pieces of as-made oxysulfide samples between 100 and 300 K using a homemade DC four-probe instrument. These measurements revealed the as-made materials to be semiconducting (Figure S1), suggesting they should be classified as Mott−Hubbard-type insulators. No measurements were made on reduced or fluorinated materials as these could not be sintered without decomposition.

Results and Discussion

Compositions and Crystal Structures. Crystal Structure and Mn-Deficiency in $Sr_4Mn_{3-\gamma}O_{7.5-\epsilon}Cu_2S_2$. The crystal structures of $Sr_4Mn_3O_{7.5}Cu_2S_2$ and $Sr_4Mn_3O_{7.5}Cu_2Se_2$ have been reported,[8] derived from powder X-ray diffraction data. Examination of the single-crystal diffraction data for crystals of $Sr_4Mn_3O_{7.5}Cu_2S_2$ did not show any systematic absences other than those corresponding to a body-centered tetragonal lattice suggesting space groups *I*4, $I\bar{4}$, *I*4/*m*, *I*422, *I*4*mm*, *I*4/*mmm*, or $I\bar{4}m2$. The lattice parameters of 3.9046(1) and 34.468(1) Å together with the Sr/Mn/Cu/S ratio of 2:1.5:1:1.1 (with estimated standard deviations of 10% on these values) obtained from EDX measurements suggested that the material was isostructural with the reported $Sr_4Mn_3Cu_2O_{7.5}S_2$.[8] Structure solution in *I*4/*mmm* by Direct Methods confirmed this. Initial refinement was performed using isotropic atomic displacement parameters (ADP) and led to *R*-factors R1(F^2) = 0.0603 and wR2(F^2) = 0.1217. The isotropic ADP of O2 located in the central MnO_2 layer at (1/2 0 0) was a factor of 8 larger than those of the other oxygen atoms. Consequently the fractional site occupancy of the O2 site was refined, converging to 0.71(1), consistent with the earlier report.[8] Refinement of the occupancy factors of the other sites showed that the Mn2 site, also located in the central MnO_2 layer, was also slightly deficient. Refinement with anisotropic ADPs for all atoms produced a very large U_{22} (0.17 Å^2) for O2 (1/2 0 0), and a marginally superior refinement against SXRD data was achieved with this atom located on a split site (1/2 ±*y* 0) with $y = 0.070(8)$ and modeled as a pair of fairly isotropic and overlapping ellipsoids (U_{22} of 0.08(3) Å^2) with their centers displaced by 0.3 Å from the ideal position. A similar model has been required in the closely related materials $Sr_4Mn_3O_{7.56}Cl_2$,[27,28] $Sr_4Co_3O_{7.5}Cl_2$,[29] and $Pb_4Fe_3O_8X$ (X = Cl,

(20) Otwinowski, Z.; Minor, W. DENZO-SMN. In *Macromolecular Crystallography, Part A*; Carter, C. W., Jr., Sweets, R. M., Eds.; Methods of Enzymology, Vol. 276; Academic Press: New York, 1997.
(21) Busing, W. R.; Levy, H. A. *Acta Crystallogr.* **1957**, *10*, 180.
(22) Altomare, A.; Burla, M. C.; Camalli, M.; Cascarano, G. L.; Giacovazzo, C.; Guagliardi, A.; Moliterni, A. G. G.; Polidori, G.; Spagna, R. *J. Appl. Crystallogr.* **1999**, *32*, 115.
(23) Sheldrick, G. M. *SHELX97: Programs for Crystal Structure Analysis* (Release 97-2); University of Göttingen: Germany, 1997.
(24) Larson, A. C.; Von Dreele, R. B. *General Structure Analysis System (GSAS)*; Los Alamos National Laboratory Report LAUR 86-748; Los Alamos National Laboratory: Los Alamos, NM, 2000; http://www.ccp14.ac.uk/ccp/ccp14/ftp-mirror/gsas/public/gsas/manual/GSASManual.pdf.
(25) Toby, B. H. *J. Appl. Crystallogr.* **2001**, *34*, 210.
(26) Wilson, A. J. C., Ed. *International Tables for Crystallography*; Kluwer Academic Publishers: Dordrecht, The Netherlands, 1995; Vol. C.

Table 1. Results of Refinements of the Structures of As-Made Mn-Rich Samples of $Sr_4Mn_{3-\gamma}O_{7-\epsilon}Cu_2S_2$ against SXRD Data and PND Data

formula	$Sr_4Mn_{2.94(2)}O_{7.42(5)}Cu_2S_2$		$Sr_4Mn_{2.91(1)}O_{7.40(1)}Cu_2S_2$
radiation	Mo Kα, $\lambda = 0.71073$ Å		neutron
instrument	Enraf Nonius FR590 κCCD		POLARIS
physical form	black plate		black powder
T/ K	293		295
crystal system		tetragonal	
space group		*I*4/*mmm*	
formula weight	821.8		820.04
a/Å	3.9046(1)		3.87248(3)
c/Å	34.468(1)		34.5892(4)
V/Å^3	525.50(3)		518.70(1)
Z	2		2
ρ_{calc}/Mg m^{-3}	5.193		5.250
independent reflections	568		–
no. of variables	31		73
χ^2	1.05		2.290
$R1$	0.0312		–
wR2	0.074		–
R_{wp}	–		0.0196
R_{F2}	–		0.044

Br)[30] in which the central oxygen atoms in triple perovskite layers similar to those described here are well described by split-site models, and in the $n = 3$ R−P oxide $Ca_4Mn_2FeO_{9.75}$.[15] The total occupancy of manganese and oxygen sites corresponded to the formula $Sr_4Mn_{2.94(2)}O_{7.42(5)}Cu_2S_2$ with all the vacancies in the central of the three sheets of nominal composition MnO_2. Refinement results are given in Table 1. Refined atomic parameters are presented in Table S1, and selected bond distances and angles are presented in Table S2. The structure is shown in Figure S2.

Further investigation of the structures was carried out using PND measurements on a series of oxysulfide samples in order to investigate the Mn and oxide ion deficiencies. In these analyses, carried out using data from POLARIS, all atoms were treated as anisotropic apart from Mn and S, which have coherent scattering lengths of relatively small magnitude (−3.73 fm and 2.847 fm, respectively)[26] compared with the average magnitude for the compound (5.6 fm), and the O2 site was treated as a highly anisotropic unsplit site for ease of comparison of the ellipsoid parameters between samples. A preliminary powder sample prepared with the ideal stoichiometry "$Sr_4Mn_3O_{7.5}Cu_2S_2$" contained excess MnO (mole fraction 0.09(1)), and the refined composition of the sample ($Sr_4Mn_{2.93(1)}O_{7.32(1)}Cu_2S_2$) was fairly consistent with the single-crystal result and with the amount of surplus MnO. While an apparent Mn deficiency indicated solely by neutron diffraction could conceivably be a consequence of substitution of Cu^{2+} ions on the Mn site (the scattering lengths are −3.73 fm for Mn and +7.718(4) fm for Cu[26]), this possibility is ruled out by the agreement of the PND and SXRD results. Subsequently, the introduction of intentional MnO deficiency into the reactants in an attempt to produce single-phase material resulted reliably in even greater deficiency at the Mn2 and O2 sites. A sample with reactant stoichiometry "$Sr_4Mn_{2.96}O_{7.46}Cu_2S_2$" produced a product with a refined composition of $Sr_4Mn_{2.91(1)}O_{7.40(1)}Cu_2S_2$ with the required 0.07(1) mol equiv of MnO evident in the refinement (the refinement is shown in Figure 2 and the refined structure in Figure 3). A further sample with reactant stoichiometry "$Sr_4Mn_{2.90}O_{7.35}Cu_2S_2$" produced a refined composition of $Sr_4Mn_{2.77(1)}O_{7.27(1)}Cu_2S_2$ with the additional Mn accounted for by 0.11(1) mol equiv of MnO. These two samples ($Sr_4Mn_{2.91}O_{7.40}Cu_2S_2$ and $Sr_4Mn_{2.77}O_{7.27}Cu_2S_2$) were respectively the "Mn-rich" and "Mn-poor" oxysulfides

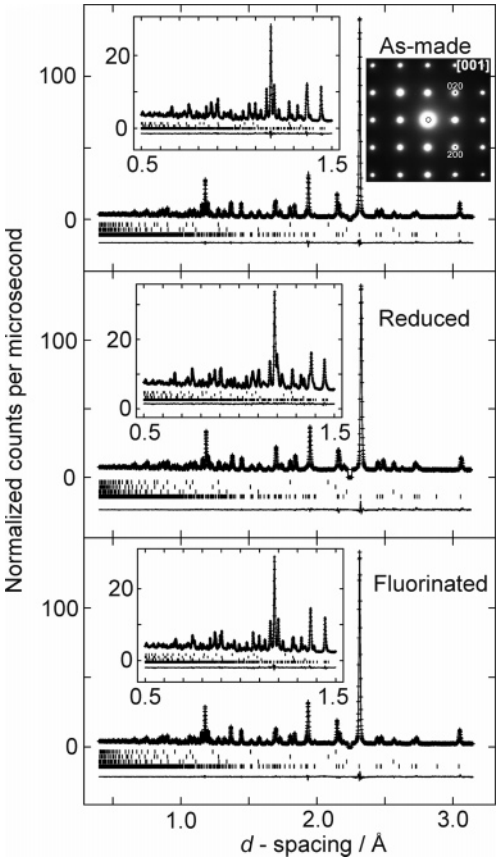

Figure 2. Results of Rietveld refinement of the structures of a series of Mn-rich oxysulfides against POLARIS data. (Top) $Sr_4Mn_{2.91(1)}O_{7.40(1)}Cu_2S_2$. (Middle) $Sr_4Mn_{2.91}O_{7.05(1)}Cu_2S_2$. (Bottom) $Sr_4Mn_{2.91}O_{7.40}F_{0.06(1)}Cu_2S_2$. The diffractograms collected by the 145° detector bank are shown. The data (points), fit (line), and difference plots (lower line) are shown. The reflection positions for the phases used in the refinement are shown. From bottom: The oxysulfide phase (99.9 mol %), MnO (0.08 mol %), Cu (0.02 mol %). For the oxidized (i.e., fluorinated) and reduced samples the vanadium sample container was also included as a phase in the refinement. The origin of an impurity peak at $d = 2.25$ Å with an intensity around 0.7% of that of the most intense peak in the main phase was not identified and was excluded from the refinement. The position of this peak was invariant under oxidation or reduction, and it was eliminated in subsequent syntheses. The electron diffraction patterns of the as-made sample $Sr_4Mn_{2.91(1)}O_{7.40(1)}Cu_2S_2$ ([001] zone shown; see also Figure S3) were devoid of any features suggestive of ordering of vacancies within the central MnO_2 sheets.

(27) Knee, C. S.; Weller, M. T. *Chem. Commun.* **2002**, 256.
(28) Knee, C. S.; Zhukov, A. A.; Weller, M. T. *Chem. Mater.* **2002**, *14*, 4249.
(29) Loureiro, S. M.; Felser, C.; Huang, Q.; Cava, R. J. *Chem. Mater.* **2000**, *12*, 3181.
(30) Knee, C. S.; Weller, M. T. *J. Mater. Chem.* **2001**, *11*, 2350.

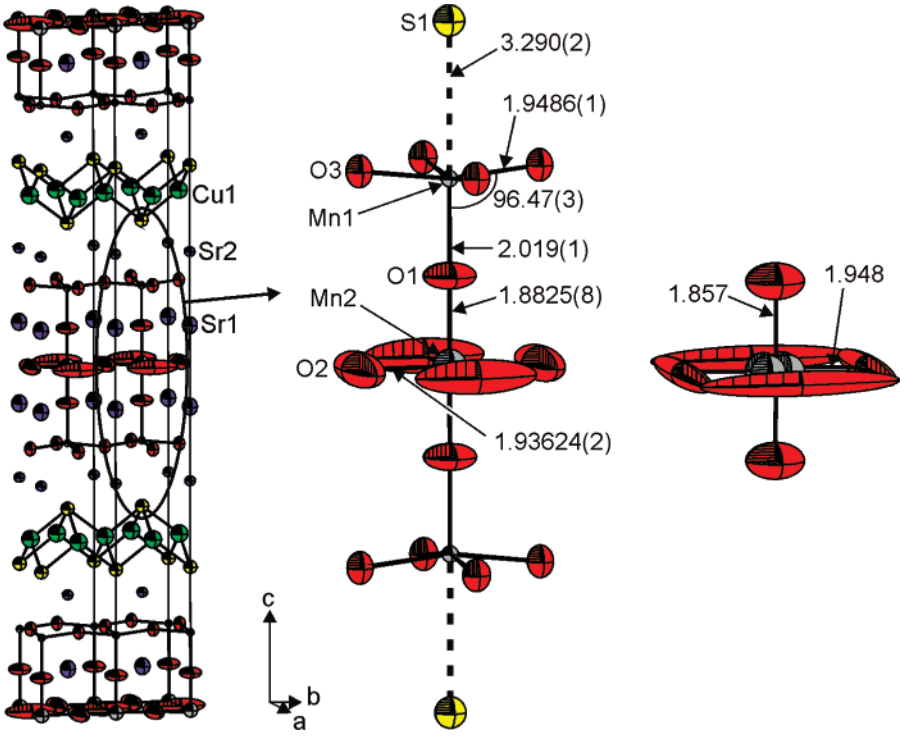

Figure 3. Crystal structure of $Sr_4Mn_{2.91(1)}O_{7.40(1)}Cu_2S_2$ from refinement against POLARIS PND data; 99% displacement ellipsoids are shown; selected bond lengths are given in Å and angles are given in degrees. The geometry of the central part of the oxide layer of the reduced $Sr_4Mn_{2.91}O_{7.05(1)}Cu_2S_2$ with a split Mn2 site and enlarged O2 displacement ellipsoids is shown for comparison. (In this case distances are measured from the O sites to the center of the octahedron.)

used for subsequent oxidation and reduction reactions described below. Attempts to intentionally synthesize the most Mn-deficient material phase pure resulted in significant quantities of impurities which were not identified. It is clear from these results that the compound is intrinsically deficient in MnO and may indeed exist in equilibrium with the binary as we have been unable to synthesize samples which are completely devoid of MnO according to PND measurements. The effects of the Mn deficiency on the magnetic properties are discussed below. A small amount of elemental copper was identified in the PND patterns, indicating that the Cu site may be around 1% deficient (deficiencies of up to 25% are accommodated in compounds with similar copper sulfide layers[9,11]); however, the level of deficiency is smaller than can reliably be determined by refinement, so the fractional occupancy of the Cu site was fixed at 1.0. Electron diffraction measurements (Figures 2 and S3) on the Mn-rich powder sample $Sr_4Mn_{2.91(1)}O_{7.40(1)}Cu_2S_2$ did not reveal any superstructure resulting from ordering of vacancies within the central MnO_2 sheets. The refinement results for the oxysulfide samples including refined atomic parameters and selected bond lengths and angles are presented in Tables S3−S8.

Crystal Structure of $Sr_4Mn_3O_{7.5}Cu_2Se_2$. The oxyselenide was synthesized phase pure according to PXRD measurements. Refinement of the structure against PND data confirmed that the oxyselenide and the oxysulfide are isostructural. MnO was identified as a much less significant impurity than in the oxysulfide, suggesting that the deficiency in the Mn2 site in the central MnO_2 layer may be 1% (a deficiency that cannot be reliably be determined by refinement of the fractional occupancy of the site). The refined compositions of two different oxyselenide samples, both measured on POLARIS and used respectively for subsequent reduction and fluorination reactions were $Sr_4Mn_3O_{7.53(1)}Cu_2Se_2$ and $Sr_4Mn_3O_{7.56(1)}Cu_2Se_2$. The uncertainly in the O2 site occupancy may be underestimated due to correlations between the site occupancy and the parameters describing the large displacement ellipsoid for O2. Furthermore, a systematic correlation between the site occupancy and the displacement parameters rather than adventitious incorporation of additional oxygen from the silica tube may be responsible for the apparent O-rich nature of these compounds. However, it is clear that these two oxyselenide samples differ slightly in their lattice parameters and in other structural parameters, suggesting a narrow phase width for this compound. In our comparisons of as-made with reduced and oxidized oxysulfides and oxyselenides we have taken care to compare samples derived from the same batch of as-made material. Our synthetic results for the oxyselenides are consistent with the previous report of this compound[8] and show that, unlike results for the oxysulfide, there is no evidence for significant Mn deficiency in the oxyselenide. The refinement results for the oxyselenide are presented in Table S9. Refined atomic parameters are tabulated in Table S10, and selected bond distances and angles are listed in Table S11.

Fluorinated Materials. Fluorination of the Mn-rich oxysulfide sample of refined composition $Sr_4Mn_{2.91}O_{7.40}Cu_2S_2$ resulted in a decrease of the *a* lattice parameter by 0.17%, an increase of the *c* lattice parameter by a similar percentage, and a resulting decrease in cell volume of 0.15%, but otherwise negligible change in the PXRD pattern. Rietveld refinement of the structure was carried out against POLARIS PND data with the assumption that the Mn and O content of the fluorinated phase was the same as that of the starting material. Refinement of the fractional occupancy of the O2 site resulted in an increase of scattering

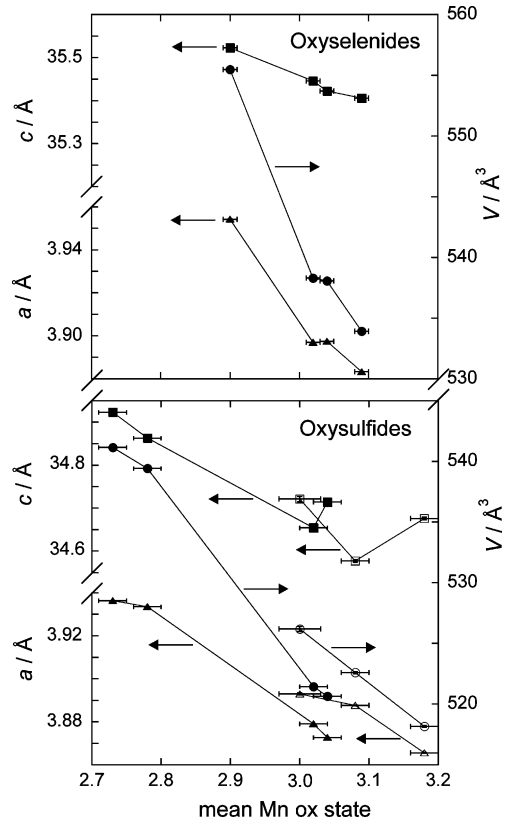

Figure 4. Correlation of the tetragonal lattice parameters *a* (triangles) and *c* (squares) and the unit cell volume (circles) with the mean Mn oxidation state derived from the refined composition for reduced and fluorinated oxysulfides (lower) and oxyselenides (upper). For the oxysulfides, which have variable Mn content, closed symbols represent Mn-rich compositions and open symbols represent Mn-poor compositions. Similar scales are used on each axis for both series of compounds. Lines are guides to the eye.

density at that site. Although F and O are indistinguishable using neutron diffraction (scattering lengths of 5.805(4) fm and 5.65(1) fm, respectively[26]), we assume that the increase in scattering density may be attributed to the intercalation of fluorine with fluoride ions occupying the O2 site. The refined formula was $Sr_4Mn_{2.91}O_{7.40}F_{0.06(1)}Cu_2S_2$, and this small degree of fluorination has a significant effect on the magnetic properties as discussed below. There was no increase in the phase fraction of the MnO impurity phase. Fluorination of the Mn-poor oxysulfide of refined composition $Sr_4Mn_{2.77}O_{7.27}Cu_2S_2$ using a three-step approach with exposure to a total of 0.45 mole of XeF_2 per mole of oxysulfide resulted in a compound with a refined composition of $Sr_4Mn_{2.77}O_{7.27}F_{0.27(1)}Cu_2S_2$. In this case, the lattice parameter *a* decreased by 0.57%, and *c* increased by 0.29%, resulting in a volume decrease of 0.85%. The changes in lattice parameters on fluorination and reduction are shown in Figure 4. For the fluorination of both the Mn-rich and Mn-poor oxysulfides, the percentage decreases in cell volume per intercalated fluorine are similar within experimental uncertainty: 2.5(4)% and 3.2(1)%, respectively. However, the penalty for a greater degree of fluorination in the Mn-poor case was partial decomposition and the formation of 0.18 mol equiv of SrF_2. Chemical analysis of the sample (ICP method, Intertek Caleb Brett) produced a total fluorine content of 1.1 ± 0.1% by mass, fairly consistent with the expected 1.4% by mass based on the refined composition and the level of SrF_2 impurity. Attempted analysis of the fluorinated materials using solid-state ^{19}F NMR spectroscopy suggested that the resonance from fluorine was too broad to be observed, presumably due to rapid paramagnetic relaxation of the resonance. Fluorination of the Mn-poor material results in significant changes in the magnetic ordering as described below. Fluorination of an oxyselenide sample of composition $Sr_4Mn_3O_{7.53}Cu_2Se_2$ resulted in a product with refined composition of $Sr_4Mn_3O_{7.53}F_{0.20(1)}Cu_2Se_2$ which showed a decrease in cell volume per intercalated fluorine of 4.1(2)%, comparable with the volume decreases observed for comparable levels of fluorination in the oxysulfides. The volume decrease presumably results from the decrease in Mn−O bond lengths on oxidation.

Reduced Materials. Refinement of the structures of the reduced materials against PND data showed that the fractional occupancy of the O2 site had decreased significantly. Two reduction reactions applied to the Mn-rich oxysulfide of refined composition $Sr_4Mn_{2.91}O_{7.40}Cu_2S_2$ produced reduced materials with refined compositions $Sr_4Mn_{2.91}O_{7.05(1)}Cu_2S_2$ and $Sr_4Mn_{2.91}O_{6.97(1)}Cu_2S_2$. TGA analysis (Figure S4), in which the mass change on heating to 1000 °C of the second of these reduced products was compared with the mass change of the parent, placed a lower bound on the difference in their oxide contents of 0.2 oxide ions per formula unit. However, the reduced materials are highly air-sensitive at room temperature, and partial oxidation likely occurs during loading of the sample in the instrument. Reduction of the Mn-poor oxysulfide of refined composition $Sr_4Mn_{2.77}O_{7.27}Cu_2S_2$ yielded a reduced product of refined composition $Sr_4Mn_{2.77}O_{7.16(2)}Cu_2S_2$. Reduction of the oxyselenide $Sr_4Mn_3O_{7.56}Cu_2Se_2$ resulted in a product with a refined composition of $Sr_4Mn_3O_{7.35(2)}Cu_2Se_2$. Because of the intrinsic MnO deficiency in the oxysulfides, the reduced oxysulfide materials are extremely anion poor in the central layer (approximately 50% occupancy of the O2 site in the most reduced materials), and refinements against PND data showed that the disorder in the layer increased significantly on reduction. The reduced Mn-rich oxysulfide and reduced oxyselenide samples were modeled satisfactorily with O2 placed on its ideal site and modeled with an extremely anisotropic displacement ellipsoid (i.e., there was no improvement in the agreement factors if the split O2 model used in the SXRD refinement was chosen). For the most Mn-deficient reduced oxysulfide material it was necessary to use the split-site model because otherwise the extreme anisotropy of the ellipsoid could not be accommodated in GSAS. In all the reduced oxysulfides the Mn2 site in the central layer was best modeled as a four-fold split site with the atom located at (x x 0) with $x \approx 0.06$, i.e., displaced by about 0.2 Å from the ideal site occupied in the parent and fluorinated materials. In the case of the oxyselenides, which are intrinsically less anion- and cation poor in the central layer, Mn2 was modeled using an unsplit site. In Figure 4, the trends in lattice parameters derived (for greatest comparative accuracy) from refinement against PXRD data show that on reduction both *a* and *c* increase, reflecting reduction of Mn and consequently longer Mn−O bond lengths. For the range of reduced materials investigated, the percentage increases in cell volume per oxygen removed from the central "MnO_2" layer in the as-made materials are 10 ± 1% for the Mn-rich oxysulfides, 5 ± 1% for the Mn-poor oxysulfides, and 15 ± 2% for the oxyselenides.

Structural Trends. All the refinements of the reduced materials show both a decrease in the fractional occupancy of

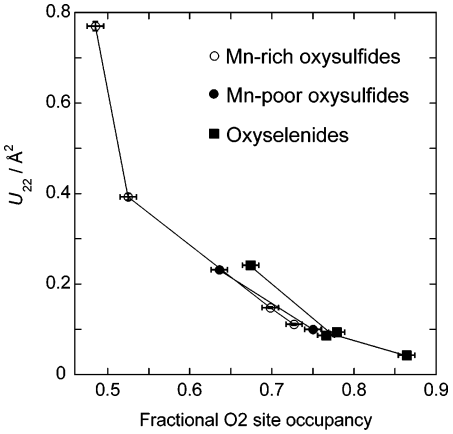

Figure 5. Correlation of the large U_{22} parameter for O2 with the fractional occupancy of the O2 site for oxysulfide and oxyselenide samples measured on POLARIS. O2 was placed on its ideal (1/2 0 0) site and modeled with a highly anisotropic ellipsoid; U_{22} measures displacement perpendicular to the Mn−O bond. The lines link points derived from analysis of samples derived from the same parent and are guides to the eye.

the anion site O2 in the central "MnO_2" layer *and* an increase in the size of the displacement ellipsoid for that site. Although these parameters are no doubt correlated, the sense in which they both change show that they are not compensating for one another in these cases. Similarly, fluorination proceeds with an increase in fractional occupancy of the O2 anion site and a decrease in the size of the displacement ellipsoid. The evolution of the displacement ellipsoids in the central layer with the fractional occupancy of the anion sites is shown graphically in Figure 5 and pictorially in Figures 3 and S5. The absolute values of the displacement parameters of the other atoms in the structure were found to be almost invariant with composition, while the displacement parameters of the atoms O2 and Mn2 in the central layer were strongly correlated with composition. The smooth variation depicted in Figure 5 suggests that the anion-site occupancies refined from the PND data are reliable.

Significant structural changes on oxidation or reduction are confined to the central MnO_2 layer. However, the effects of the topotactic reactions are evident in the other parts of the structure. Figure 6 shows the changes in the coordination environment of the Mn1 ion located in the outer parts of the oxide slab as a function of the refined anion occupancy in the central layer for Mn-rich and Mn-poor oxysulfides and oxyselenides, all measured on the POLARIS diffractometer. The smooth variation of the bond lengths with refined composition suggests that the compositions determined by PND are reliable. Furthermore, the changes in the coordination environment of Mn1, which is not directly coordinated by O2, suggests that this ion, as well as the Mn2 ion in the central layer, is partially reduced or oxidized during the topotactic transformations. For example, in the reduction of $Sr_4Mn_{2.91}O_{7.40}Cu_2S_2$ to $Sr_4Mn_{2.91}O_{7.05}Cu_2S_2$ the compositional refinement suggests that the Mn ions gain 0.70 ± 0.04 electrons between them on reduction. Bond valence sum (BVS) analysis using the EUTAX package[31] applied to Mn1 suggests that the oxidation state of each Mn1 is reduced by 0.11; therefore, the oxidation state of Mn2 should be reduced by 0.52, taking into account the incomplete

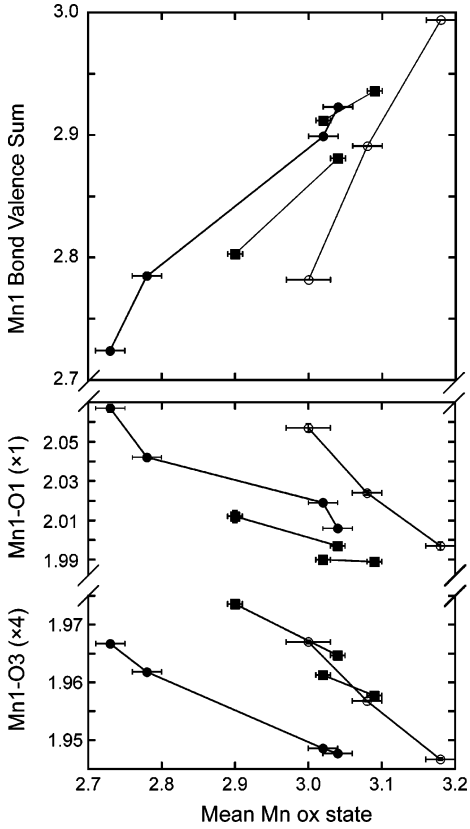

Figure 6. Correlation of the Mn1−O bond lengths and the corresponding calculated bond valence sum for Mn1 with the mean Mn oxidation state obtained from Rietveld refinements against POLARIS PND data. Mn-rich oxysulfides (closed circles), Mn-poor oxysulfides (open circles), and oxyselenides (closed squares) are shown. Lines are guides to the eye linking reduced and oxidized samples with their as-made parents.

occupancy of this site. BVS calculations cannot meaningfully be carried out for Mn2 in the disordered layer and should generally be used with caution for structures with relatively few structural variables. In this case the comparative BVS values (Figure 6) are consistent with a slight change in oxidation state for Mn1 on fluorination or reduction.

Magnetic Ordering. Magnetic Susceptibility Measurements. The magnetic susceptibilities of the Mn-rich oxysulfides derived from $Sr_4Mn_{2.91}O_{7.40}Cu_2S_2$ are shown as functions of temperature under ZFC and FC conditions in Figure 7. Two features are apparent in the measurement of the parent oxysulfide. First, there is a broad susceptibility maximum at 90 K which is identified, from low-temperature PND measurements (see below), with long-range antiferromagnetic ordering and which we designate as T_N. Second, at lower temperatures the ZFC and FC curves diverge in a manner suggestive of a glassy component to the magnetism. The fluorination and reduction reactions have a very significant effect on the magnetic susceptibility. The fluorinated sample of refined composition $Sr_4Mn_{2.91}O_{7.40}F_{0.06}Cu_2S_2$ has a T_N of 100 K, i.e., 10 K higher than in the compound from which it was derived. Reductions of the same parent material to refined compositions of $Sr_4Mn_{2.91}O_{7.05}Cu_2S_2$ and $Sr_4Mn_{2.91}O_{6.97}Cu_2S_2$ resulted in no apparent maximum in the susceptibility. Similar trends are apparent in analysis of the Mn-poor materials; in this case neither the Mn-poor parent $Sr_4Mn_{2.8}O_{7.25}Cu_2S_2$ nor its reduction product shows a susceptibility maximum ,but a distinct T_N of 110 K is obtained on fluorination ($Sr_4Mn_{2.77}O_{7.27}F_{0.27}Cu_2S_2$) (Figure S6).

(31) Brese, N. E.; O'Keeffe, M. *Acta Crystallogr., Sect. B: Struct. Sci.* **1991**, *47*, 192.
(32) Goodwin, A. L.; Tucker, M. G.; Dove, M. T.; Keen, D. A. *Phys. Rev. Lett.* **2006**, *96*, 047209.

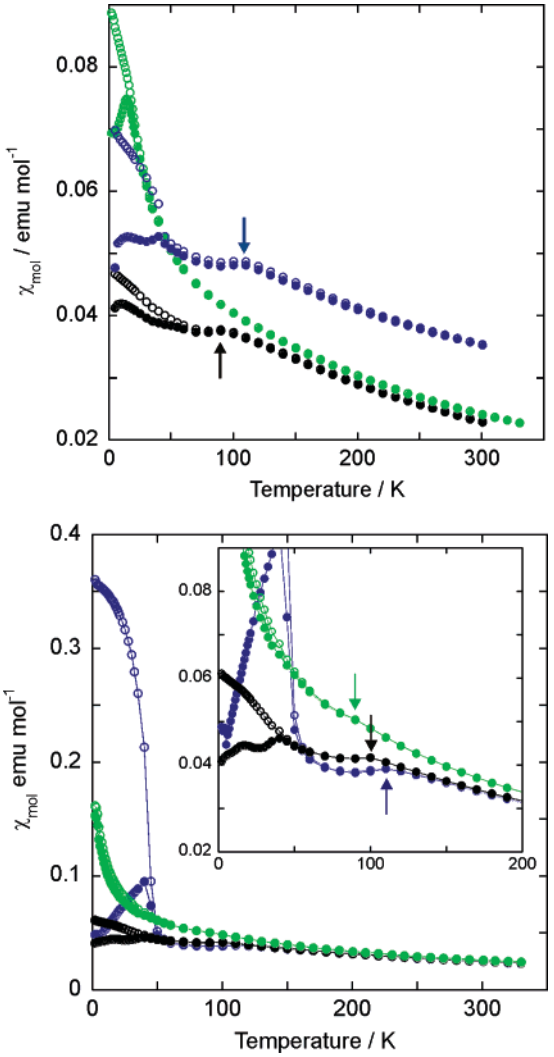

Figure 7. (Upper) Magnetic susceptibilities of Mn-rich oxysulfides: as-made $Sr_4Mn_{2.91}O_{7.40}Cu_2S_2$ (black), reduced $Sr_4Mn_{2.91}O_{7.05}Cu_2S_2$ (green), and oxidized $Sr_4Mn_{2.91}O_{7.40}F_{0.06}Cu_2S_2$ (blue). (Lower) Oxyselenides: as-made $Sr_4Mn_3O_{7.53}Cu_2Se_2$ (black), reduced $Sr_4Mn_3O_{7.35}Cu_2Se_2$ (green), and oxidized $Sr_4Mn_3O_{7.53}F_{0.20}Cu_2Se_2$ (blue). Samples were measured under zero-field-cooled (ZFC) (closed symbols) and field-cooled (FC) (open symbols) conditions in a measuring field of 0.01 T. Discernible maxima equated with the Neél temperatures, T_N, are indicated by arrows.

In the case of the oxyselenides, which are fully stoichiometric in Mn and consequently also less oxide deficient than the sulfides, the broad susceptibility maximum is not quite eradicated on reduction (Figure 7). T_N values are 90 ± 5 K for $Sr_4Mn_3O_{7.35}Cu_2Se_2$, 100 ± 2 K for $Sr_4Mn_3O_{7.56}Cu_2Se_2$, and 110 ± 2 K for $Sr_4Mn_3O_{7.53}F_{0.20}Cu_2Se_2$. T_N is correlated with the strength of the superexchange interactions and hence would be expected to increase with contracting Mn−O distances (Figure 6) on oxidation. At 5 K (i.e., below the divergence in the ZFC and FC curves) the magnetization isotherms for all compounds exhibit hysteresis and are displaced from the origin (Figure S7), suggesting that the divergence in the ZFC and FC curves is due to spin-glass behavior. As the mean Mn oxidation state decreases, the magnetization isotherms measured at 5 K after field cooling exhibit a decreased thermal-remanent magnetization, a decreased displacement from the origin, and a decreased hysteresis. This coincides with the smaller divergence of the ZFC and FC susceptibilities on reduction. In the fluorinated

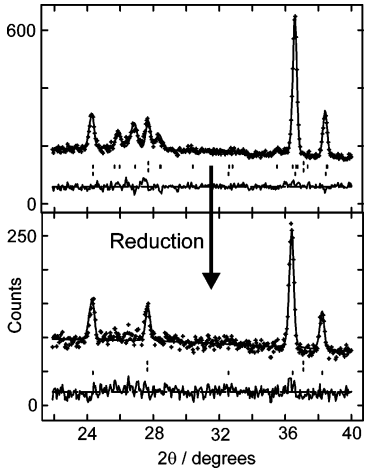

Figure 8. Portions of the PND patterns for the Mn-rich oxysulfide $Sr_4Mn_{2.91}O_{7.40}Cu_2S_2$ (upper) and its reduction product $Sr_4Mn_{2.91}O_{7.05}Cu_2S_2$ (lower) obtained at 5 K using the diffractometer D2B. The lines show the fits obtained by Rietveld refinement against the data of the structural model, the magnetic model depicted in the inset to Figure 9 for the as-made material, and the crystal and magnetic structure of the MnO impurity.[32] On reduction there are no apparent magnetic Bragg peaks associated with the oxysulfide phase.

oxyselenide there is the suggestion of weak ferromagnetic behavior in the ZFC/FC susceptibility curves (Figure 7); this may arise from spin canting although it is possible that this is partly an artifact of the large displacement of the low-temperature magnetization isotherms from the origin and the large hysteresis.

Neutron Diffraction Measurements. Powder neutron diffraction investigations below T_N carried out on the diffractometer D2B at ILL showed no structural changes but showed the appearance of new Bragg peaks (Figure 8) consistent with antiferromagnetic ordering on a cell with lattice parameters of $\sqrt{2}a \times \sqrt{2}a \times c$ relative to the structural cell. In the sample $Sr_4Mn_{2.91}O_{7.40}Cu_2S_2$ these peaks were absent at 125 K (above $T_N = 90$ K) and present at 75 K and below. The Mn-rich parent oxysulfides and all the oxyselenide materials exhibited similar patterns of magnetic Bragg peaks. Several models were considered to account for this; the only model that successfully accounts for the observed scattering is shown in Figure 9. The Mn moments in the outer layers of the perovskite block are aligned along the tetragonal axis and are arranged antiferromagnetically to their four nearest neighbors in the layer and antiferromagnetically to their neighbor on the opposite side of the perovskite block. This model is consistent with the expected superexchange interactions between d^4 Mn^{3+} ions in the geometries shown in Figure 3. Mn1 in square pyramidal coordination with a long apical bond to O1 and four shorter bonds to O3 has its $d_{x^2-y^2}$ orbital as its most antibonding and empty d orbital, whereas d_{z^2} is less antibonding and is occupied. Mn2, nominally in a distorted octahedral coordination environment, has short apical bonds to the fully occupied O1 and longer bonds to the partially occupied O2 site in the central "MnO_2" sheet, making d_{z^2} the most σ-antibonding and empty d orbital. Thus, the dominant σ-superexchange between the occupied d_{z^2} orbitals on two Mn1 ions on opposite side of the oxide slab is mediated by the empty d_{z^2} orbital on Mn2 and is hence antiferromagnetic following the analysis of refs 33 and 34. The moment of Mn2 is frustrated by these σ superexchange interactions which attempt to align Mn2 ferromagnetically to

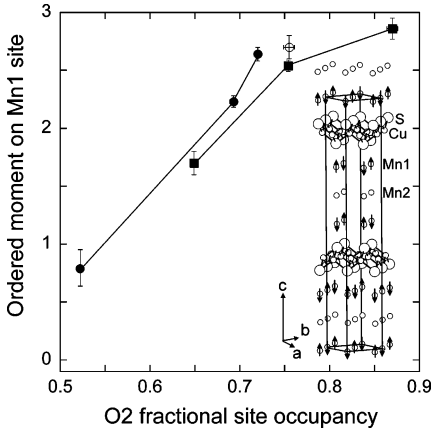

Figure 9. Correlation of the ordered moment per Mn1 ion in the outer part of the oxide layer with the fractional site occupancy of the O2 anion site in the central layer which is a measure of the composition. Several Mn-rich oxysulfides (closed circles) and oxyselenides (closed squares) with the magnetic structure shown in the inset are included. The as-made Mn-poor oxysulfide shows a different pattern of magnetic Bragg scattering (see Figure 10), but its fluorination product is included in this figure (open circle). The magnetic unit cell is depicted; oxide and strontium ions are omitted for clarity.

both neighboring Mn1 ions.[33] The π-type superexchange interactions involving the singly occupied d_{xz} and d_{yz} orbitals on Mn1 and Mn2 ions should align Mn2 antiferromagnetically to both Mn1 ions and would hence lead to parallel alignment of the spins on the Mn1 ions on the opposite sides of the slab. In view of the observed magnetic structure, we deduce that, as expected, the π-type superexchange interactions are weaker than the σ-type interactions.

The σ- and π-type superexchange interactions between Mn2 moments within the central layer are also expected to be frustrated by the anion deficiency (and also Mn-deficiency in the case of the oxysulfides) in this layer and by the mixed-valence on the Mn2 site in the reduced and oxidized materials. The inherent frustration and disorder in these systems gives rise to the glassy component evident in the magnetic susceptibility measurements. The observed magnetic model has some qualitative similarities with the model found for the oxide-deficient $n = 3$ R−P phases $Ca_4Mn_2FeO_{9.75}$ and $Sr_4Mn_2FeO_{9.80}$. Although in these cases the magnetic ordering scheme is different in detail and the 3d cations are disordered and do not all have the same electronic configuration as those of the ions in the compounds considered here, the common features include the anion vacancy in the central layer and inherent disorder which results in glassy moments in the central layer of the perovskite block, while the two outer layers of the block participate in long-range magnetic ordering. The magnetic susceptibilities of $Ca_4Mn_2FeO_{9.75}$ and $Sr_4Mn_2FeO_{9.80}$[15] are qualitatively similar to those of the oxysulfides and oxyselenides reported here showing a broad T_N and a ZFC/FC divergence identified with spin-glass behavior at lower temperatures. In principle, a closer analogy is provided by $Sr_4Mn_3O_{7.56}Cl_2$:[28] this compound, which also contains predominantly Mn^{3+} ions, shows a very similar magnetic susceptibility to that of the oxychalcogenides reported here, and although the model for magnetic ordering could not be determined unequivocally[28] due to a lack of data at long *d*-spacings, the distribution of magnetic intensities shown in ref 28 is not inconsistent with a model similar to that reported here. As in $Ca_4Mn_2FeO_{9.75}$ and $Sr_4Mn_2FeO_{9.80}$[15] the refined values of the ordered moment in the oxysulfides and oxyselenides are lower than would be expected ($\sim 4\ \mu_B$ per Mn1 ion) if all the moments in the outer layers of the perovskite block participate in long-range magnetic ordering. In $Sr_4Mn_{2.91}O_{7.40}Cu_2S_2$ the refined magnetic moment of the Mn1 ions in the outer layers of the perovskite block is 2.23(5) μ_B. The value in the selenide analogue $Sr_4Mn_3O_{7.56}Cu_2Se_2$ is slightly larger at 2.54(5) μ_B, suggesting that the size of the ordered moment is influenced by the chemistry of the central layer. This dependence on composition and disorder was probed directly by investigating the magnetic scattering arising from the reduced and fluorinated samples and from the Mn-poor oxysulfides. For the series derived from the Mn-rich oxysulfide of composition $Sr_4Mn_{2.91}O_{7.40}Cu_2S_2$, for which the magnetic susceptibility curves are shown in Figure 7, fluorination to $Sr_4Mn_{2.91}O_{7.40}F_{0.06}Cu_2S_2$ resulted in an increase in the refined ordered moment from 2.23(5) μ_B to 2.64(6) μ_B at 5 K, which also coincides with the increase in T_N. Reduction of the same oxysulfide parent sample to $Sr_4Mn_{2.91}O_{7.05}Cu_2S_2$ resulted in an apparent absence of magnetic Bragg peaks (Figure 8), and taking into account the noise in the data, the upper-bound for the value of a long-range ordered moment was determined to be 0.8(2) μ_B, assuming the same magnetic structure as for the parent material. In this reduced material the data appear to show an extremely broad feature consistent with short-range magnetic order. The oxyselenides show a similar trend: the as-made material $Sr_4Mn_3O_{7.56}Cu_2Se_2$ has an ordered moment of 2.54(5) μ_B while the fluorinated $Sr_4Mn_3O_{7.53}F_{0.20}Cu_2Se_2$ has a larger moment of 2.86(9) μ_B, The reduced-phase $Sr_4Mn_3O_{7.35}Cu_2Se_2$ has a long-range ordered moment of 1.7(1) μ_B. The trend in the size of the long-range ordered moment with the site occupancy of the O2 anion site in the central layer, used here as a convenient measure of disorder, is shown in Figure 9. Long-range magnetic ordering giving rise to magnetic Bragg scattering is evidently extremely sensitive to the composition of these compounds. In particular in the case of the reduced materials the introduction of some Mn^{2+} ions with all d orbitals occupied at the Mn2 position will result in antiferromagnetic σ-superexchange coupling between these Mn2 ions and both neighboring Mn1 ions, reinforced by the π-superexchange. This will frustrate the long-range ordered structure adopted by the as-made and oxidized materials. The very large anion deficiency, the slight Mn deficiency, the disorder in the O2 and Mn2 positions evident in Figure 3, and the apparent slight reduction of Mn1 are expected to augment this frustration. The result is that in the highly reduced oxysulfide $Sr_4Mn_{2.91}O_{7.05}Cu_2S_2$ long-range magnetic ordering is lost. This destruction of long-range magnetic order on reduction coincides with the decrease in the hysteresis and displacement of the field-cooled magnetization isotherms and the decrease in the divergence of the ZFC and FC susceptibilities arising from the glassy magnetic component, suggesting that the effects on both the ordered and glassy magnetic components are a consequence of increasing chemical disorder on reduction. Presumably increasing chemical disorder results in a decrease in the potential energy barriers in the energy landscape of the spin-glass state, but further measurements would be required to probe this in more detail. Chemical

(33) Goodenough, J. B. *J. Phys. Chem. Solids* **1958**, *6*, 287.
(34) Kanamori, J. *J. Phys. Chem. Solids* **1959**, *10*, 87.

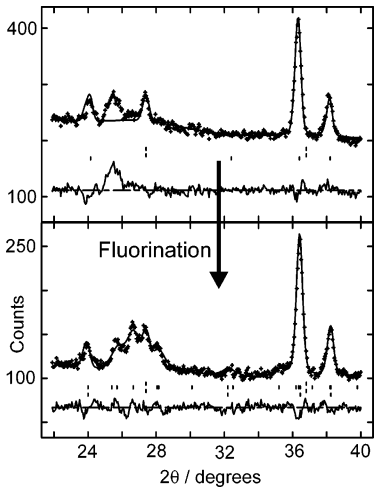

Figure 10. Portions of the PND patterns for the Mn-poor oxysulfide material $Sr_4Mn_{2.77}O_{7.27}Cu_2S_2$ (upper) and its fluorination product $Sr_4Mn_{2.77}O_{7.27}F_{0.27}Cu_2S_2$ (lower) obtained at 5 K using D2B. The lines show the fits obtained by Rietveld refinement against the structural model, the magnetic model depicted in the inset to Figure 9 for the fluorinated material, and the crystal and magnetic structure of the MnO impurity.[32]

disorder induced by 5% substitution of La^{3+} for Sr^{2+} has been reported to lead to spin-glass behavior below 200 K.[35] Finally, the as-made sample of the most Mn-deficient oxysulfide $Sr_4Mn_{2.77}O_{7.27}Cu_2S_2$ shows a different distribution of magnetic Bragg intensity from that shown by the Mn-rich oxysulfides. It has not proved possible to model this magnetic scattering unambiguously. On fluorination to $Sr_4Mn_{2.77}O_{7.27}F_{0.27}Cu_2S_2$ the familiar long-range ordered magnetic structure shown in Figure 9 is restored as shown in Figure 10. These results show the sensitivity of the magnetic ordering to the composition of the central layer.

(35) Kamihara, Y.; Naganuma, J.; Yasunaka, K.; Ishii, M.; Ueno, H.; Matoba, M. *Nippon Oyo Jiki Gakkaishi* **2003**, *27*, 666.

Conclusions

The manganese-containing oxychalcogenide relatives of the R−P phases are susceptible to both topotactic oxidation by fluorination and to reduction by reaction with sodium hydride. As far as we are aware these are the first systems in which both of these soft chemical techniques have been successfully applied to a single parent material synthesized using standard solid-state techniques. Such flexibility may conceivably have relevance in catalytic or electrode applications. The fluorinations and reductions exert a considerable influence over the detailed crystal structures of these compounds, and the magnetic ordering is very sensitive to the composition and structure.

Acknowledgment. We thank Dr. M. A. Hayward (Inorganic Chemistry Laboratory, University of Oxford) for advice, particularly concerning the topotactic reductions, Drs. A. Hewat and E. Suard (ILL, Grenoble) and Dr. R. I. Smith (ISIS facility), for assistance with the neutron diffraction investigations, Dr. N. Charnley (Department of Earth Sciences, University of Oxford) for assistance with EDX analysis. We thank the EPSRC for support under Grant GR/N18758, for the award of a studentship for G.H., and for access to the ISIS facility and ILL.

Supporting Information Available: Crystallographic data in CIF format for $Sr_4Mn_{2.94(2)}O_{7.42(5)}Cu_2S_2$ (293 K); tables of refinement results, refined atomic coordinates, and bond distances and angles from SXRD and PND refinements (Tables S1−S11); diagrams showing electrical resistivity measurements (Figure S1), crystal structure of $Sr_4Mn_{2.94(2)}O_{7.42(5)}Cu_2S_2$ showing displacement ellipsoids (Figure S2), electron diffraction patterns (Figure S3), TGA results (Figure S4), displacement ellipsoids correlated with composition (Figure S5), and further magnetic measurements (Figures S6, S7). This material is available free of charge via the Internet at http://pubs.acs.org.

JA073048M